J Mater Sci: Mater Electron **(2025) 36:727**

Sustainable synthesis and functionalization of ZnO photocatalysts using *Amphipterygium adstringens* (Cuachalalate) bark extract for the effective degradation of emerging pollutants

A. Moreno Meza[1], A. R. Vilchis-Nestor[2], and P. A. Luque[1,*]

[1] *Facultad de Ingeniería, Arquitectura y Diseño-Universidad Autónoma de Baja California, C.P. 22860 Ensenada, México*
[2] *Centro Conjunto de Investigación en Química Sustentable, UAEM-UNAM, C.P. 50200 Toluca, México*

Received: 19 November 2024
Accepted: 29 March 2025
Published online: 25 April 2025

© The Author(s), 2025

ABSTRACT

This study investigates the photocatalytic degradation of emerging pollutants (EP) using zinc oxide nanoparticles (ZnO NPs) synthesized via green chemistry. It employs *Amphipterygium adstringens* (Cuachalalate) bark extract as a natural reducing and stabilizing agent. The photocatalytic performance of the synthesized ZnO NPs was evaluated under ultraviolet (UV) light irradiation using various model compounds, including the dyes Congo Red (CR), Malachite Green (MG), Rhodamine B (RhB), Methylene Blue (MB), and Methyl Orange (MO), as well as the pharmaceutical contaminants Ibuprofen (IBU), Ciprofloxacin (CIP), and Diclofenac sodium (DCF). Characterization techniques determine the physical, chemical, and electronic properties of ZnO NPs. Ultraviolet–visible (UV–Vis) spectroscopy presents an absorbance peak at 371 nm, and the TAUC plots of each spectrum revealed band gaps of 2.948, 2.940, and 2.847 eV for 1%-ZnO NPs, 2%-ZnO NPs, and 4%-ZnO NPs, respectively. At the same time, the obtention vibration bonds through FTIR spectroscopy showed Zn–O stretching vibration at 380 cm^{-1}. X-ray diffraction (XRD) shows the crystalline structure, with average crystallite sizes of 21.6 nm, 14.19 nm, and 13.26 nm for 1%-ZnO NPs, 2%-ZnO NPs, and 4%-ZnO NPs, respectively. Finally, scanning electronic microscopy showed the morphology, which was spherical with a slight agglomeration of the particles. The photocatalytic degradation efficiency of the ZnO NPs was approximately 90% for dyes and 85% for drug contaminants. The degradation constant was determined using the equation of first-order kinetics. These promising results highlight the potential of Cuachalalate-derived ZnO NPs for efficiently remedying emerging pollutants and suggest further environmental application research, pollutants and suggest for further research in environmental applications.

Address correspondence to E-mail: pluque@uabc.edu.mx

https://doi.org/10.1007/s10854-025-14696-0

1 Introduction

In recent years, human activities, such as food production, textiles, and the pharmaceutical industries [1–3], have produced organic waste as by-products, resulting in water pollution and wastewater with highly toxic organic pollutants that are the main environmental and health problems [4–6]. Chemical pollutants known as emerging pollutants (EP) are compounds used in modern society that compromise the health of living organisms. The presence of pharmaceutical compounds in the aquatic environment is a global concern. The low concentration of compounds can affect microorganisms and increase the resistant pathogens in wastewater [7, 8]. Antibiotics are produced and utilized in large amounts, causing toxicity to water bodies [9].

For this reason, nanomaterials have attracted enormous interest due to their wide range of properties. Generally, heterogeneous photocatalysis with nano semiconductors is effective for complete degradation and can eliminate toxic organic pollution from industrial activity [10, 11]. The semiconductor nanomaterial presents unique size-dependent properties related to its high specific surface area, including localized surface plasmon resonance and quantum confinement effects [12–14]. This is because the band gap of nanomaterials is a principal factor in photocatalytic reactions.

Therefore, zinc oxide nanoparticles (ZnO NPs) are promising metal oxide semiconductor photocatalysts for several applications due to their higher quantum efficiency and rapid range of photocatalytic activity [15, 16]. ZnO NPs have a band gap of 3.37 eV in the near-ultraviolet spectrum and exhibit n-type conductivity [17]. In addition, ZnO NPs show characteristics such as high surface specificity, low toxicity, surfactant sites for specific absorption, high chemical and thermal stability, and photocatalytic activity over a broader range of ultraviolet–visible light and low cost [18–21]. The oxidation process for the superoxide radical may generate photo generation. Single excitons form coulomb interaction between electrons and holes [22].

The synthesis of ZnO NPs via the green method is an alternative to the production of ZnO NPs. Conventional processes, such as chemical synthesis, require potent chemicals that can potentially lead to environmental contamination [23, 24]. The use of plants, fruits, and bark involves several metabolites and biomolecules that contain functional groups, such as carbonyl (–CO), hydroxyl (–OH), and amines ($–NH_2$). Antioxidant molecules are considered essential for forming ZnO NPs that react with a precursor of metal ions, providing stability and surface functionality to the nanoparticles [25]. *A. adstringens* (cuachalalate), known as "cuachalalate" is an endemic plant of Mexico [26]. The bark commonly treats gastric ulcers, inflammation, colic, and gastrointestinal cancer [27].

The principal components of the cuachalalate bark are the triterpenoid acids 3α-hydroxymasticadienoic (3 MA) and masticadienoic (MA). The anacardic acids (ANA) and anacardic aldehydes are among the long-chain phenolic compounds [28]. Actuality, green synthesis has been applied using different extracts, e.g., Islam et al. and performed the green synthesis of ZnO NPs from onion (*Allium cepa L.)* waste husk, obtaining a particle size between 49 and 100 nm, resulting in an average particle size of 57.38 nm. On the other hand, Ansari et al. they synthesized ZnO NPs using *Eucalyptus globulus* leaf extract, confirming its formation by XRD, TEM, FE-SEM, and FTIR techniques. They obtained results with an average particle size of 6 ± 2 nm [29, 30].

This study innovates using a novel bark extract to synthesize and functionalize ZnO NPs for decontaminating wastewater from emerging pollutants. Specifically, IBU, DCF, and CIP degradation occur under conditions controlled for efficient drug degradation. It demonstrates effectiveness, rentability, and low cost of production.

2 Details experiments

2.1 Materials and chemicals

The bark of the cuachalalate tree (*Amphipterygium astringent*) was purchased from a local herbalist store in Querétaro, México. The zinc nitrate hexahydrate was purchased from Sigma-Aldrich. Finally, sterile ultra-pure water was utilized as a solvent.

2.2 Active compound extract

For active compound utilization, the tree bark prepared 1%, 2%, and 4% (wt/vol) extract solutions in 50 mL of sterile, ultra-pure water. The samples were stirred for 2 h and then placed in a water bath at 60 °C for 1 h. Finally, the extracts were vacuum-filtered to

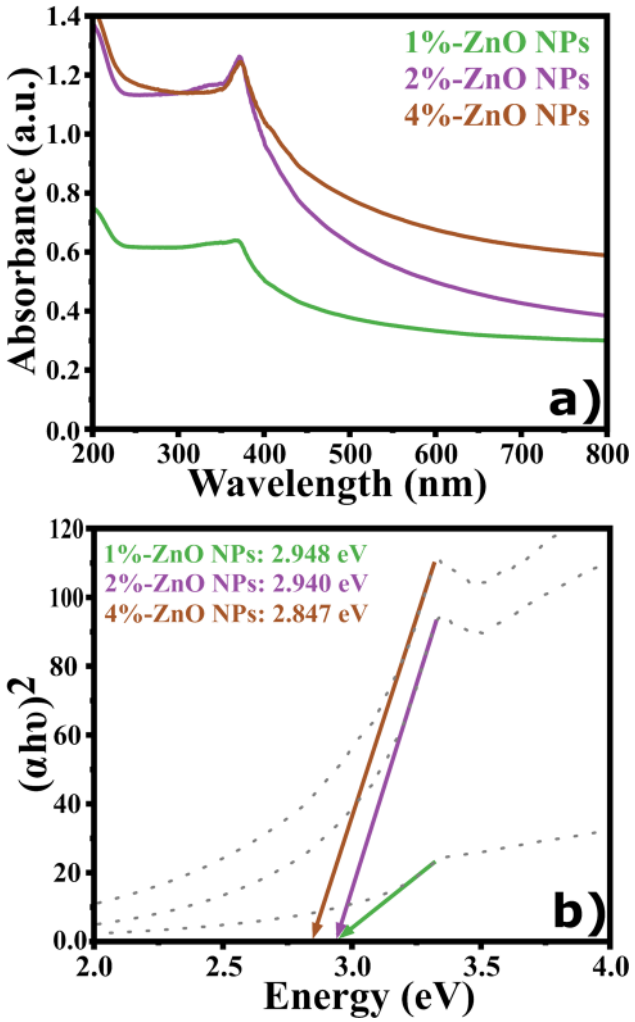


Fig. 1 **a** UV–Vis Spectre absorption, **b** Determination of the bandgap energy by TAUC plot

separate solid residues from the liquid and stored for further processing studies.

2.3 Synthesis of ZnO NPs

2 g of zinc nitrate hexahydrate was dissolved in 40 mL of the cuachalalate extract at 1%, 2%, and 4% (w/v). The solutions were stirred for one h until the Zn precursor was fully dissolved. Continuing with the reaction, the solutions were placed in a thermoregulated water bath at 60 °C for 11 h until a pasty consistency was achieved. Finally, they were subjected to heat treatment at 400 °C for one h, obtaining a grayish-white product that was passed into an agate mortar. At the end of this process, the product was stored and labeled as 1%-ZnO NPs, 2%-ZnO NPs, and 4%-ZnO

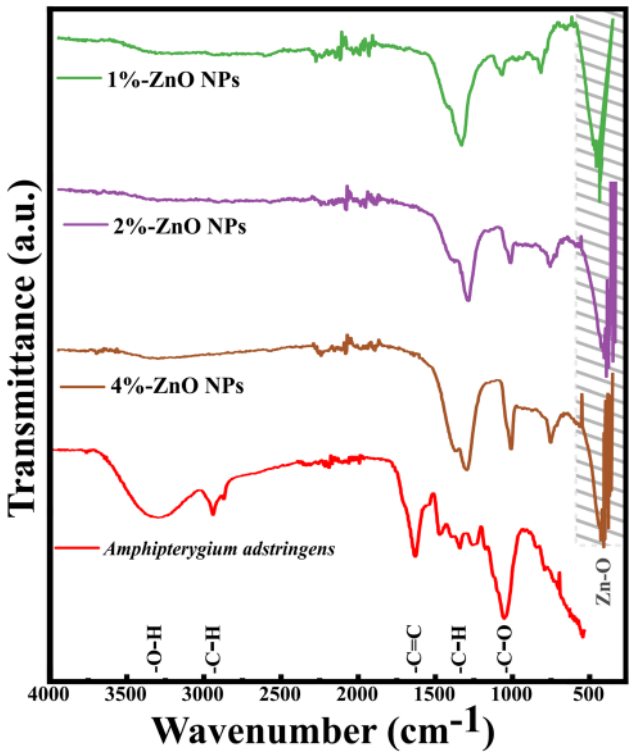


Fig. 2 Analysis FTIR of ZnO nanoparticles synthesized with percentages 1%-ZnO NPs, 2%-ZnO NPs, and 4%-ZnO NPs

NPs, corresponding to the extract concentration of 1%, 2%, and 4%, respectively. Subsequently, their characterization and the study of their photocatalytic activity were carried out.

2.4 ZnO NPs characterization

Different analytical methods were used to characterize the ZnO nanoparticles. The absorption and band gap were defined by ultraviolet–visible spectroscopy (UV–Vis), ranging from 200 to 800 nm. Fourier transform infrared spectroscopy (FTIR) analyzed the functional groups to determine the characteristics of ZnO using a Perkin Elmer Spectrum Two spectrometer; the spectrum was taken from 4500 to 350 cm^{-1}. The crystalline structure was identified by X-ray diffraction with a wavelength of 1.5406 Å (Cu Kα). Scanning electron microscopy identified the morphology and elemental composition through energy-dispersive X-ray spectroscopy (EDX). The average particle size was obtained using transmission electron microscopy with JEM- 2100 equipment.

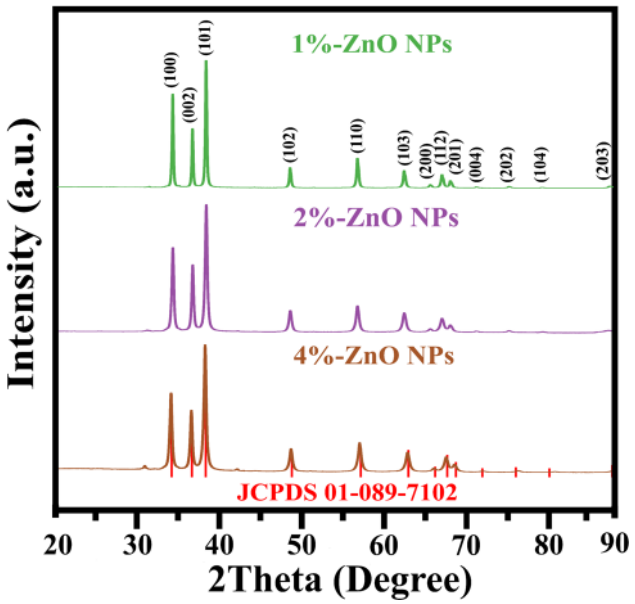


Fig. 3 Crystallographic analysis of ZnO semiconductor synthesized using different concentrations of cuachalalate bark extract

2.5 Photocatalytic activity study

In the case of photodegradation, ibuprofen, diclofenac sodium, and ciprofloxacin were used at a concentration of 20 ppm. The study used four different organic dye solutions: MB, RhB, MO, and CR, each at a concentration of 15 ppm. Degradation analyses were performed using UV light. In the experiment under UV radiation, 10 W Polaris UV- 1 C lamps with an energy of 18 mJ/cm^2 were utilized. The resulting suspension was mechanically stirred in the dark for 30 min to achieve an adsorption-resorption balance. Later, the suspensions were placed under UV radiation; during the experiment, aliquots were taken at various intervals up to 180 min. At the end, the degraded samples were measured using a UV spectrophotometer.

3 Results

3.1 Optical studies

Ultraviolet–visible molecular absorption spectrophotometry examination was completed to confirm the formation of ZnO NPs using cuachalalate extract, obtaining sharp absorbance peaks at 367, 371, and 372 nm for 1%-ZnO NPs, 2%-ZnO NPs, and 4%-ZnO NPs, as shown in Fig. 1a. These results confirm the proper formation of ZnO. The difference in absorbance corresponds to the resonance effect due to the relationship between the metal conduction electrons and the incident photons [31]. This is known as surface plasmon resonance (SPR) due to the unique properties of the ZnO NPs semiconductor and the influence of the extract used to obtain the ZnO. Figure 1b shows the values of the band gap, calculated using the TAUC approximation method, indicating energy values for 1%-ZnO NPs of 2.948 eV, 2%-ZnO NPs of 2.940 eV, and 4%-ZnO NPs of 2.847 eV despite a minimal difference. Using the energy equation and modifying it to calculate the wavelength, we obtain:

$$\lambda = \frac{hc}{E} \tag{1}$$

Therefore, the wavelengths for 1%-ZnO NPs, 2%-ZnO NPs, and 4%-ZnO NPs are 420, 422, and 435 nm, respectively.

3.2 FTIR spectroscopy analysis

The surface functionality of the ZnO NPs was demonstrated by FTIR analysis. The extract contains two main types of compounds: triterpenoids and simple aromatic compounds with aliphatic chains of 12–22 carbon atoms. However, the primary compound is the sarsasapogenin molecule. Figure 2 shows absorbance peaks at 3290, 2921, 1606, 1316, and 1029 cm^{-1}, attributed to O–H, C–H, C=C, C–H, and C–O of *A. adstringens*, corresponding to the similar spectrum reported by Arenas et al. [32]. The absorbance peaks in Fig. 2 correspond to a spectrum of ZnO NPs produced by green synthesis. This is due to the organic molecules present in the medium during the synthesis process. Organic molecules that bind to the nanoparticle surface provide stability and coating, which also help prevent agglomeration. Therefore, the observed peaks are likely from the stretching vibrations of the C=O, C–H, and C–O functional groups derived from the aromatic rings and the O–H bond of the sarsasapogenin molecule. The characteristic absorption of ZnO NPs observed at 380 cm^{-1} is attributed to the Zn–O stretching vibrations [33–37].

3.3 Determination of the XRD pattern

XRD analysis determined the crystalline structure of ZnO NPs. The obtained XRD pattern in Fig. 3 displays thirteen diffraction peaks positioned at 2θ values of

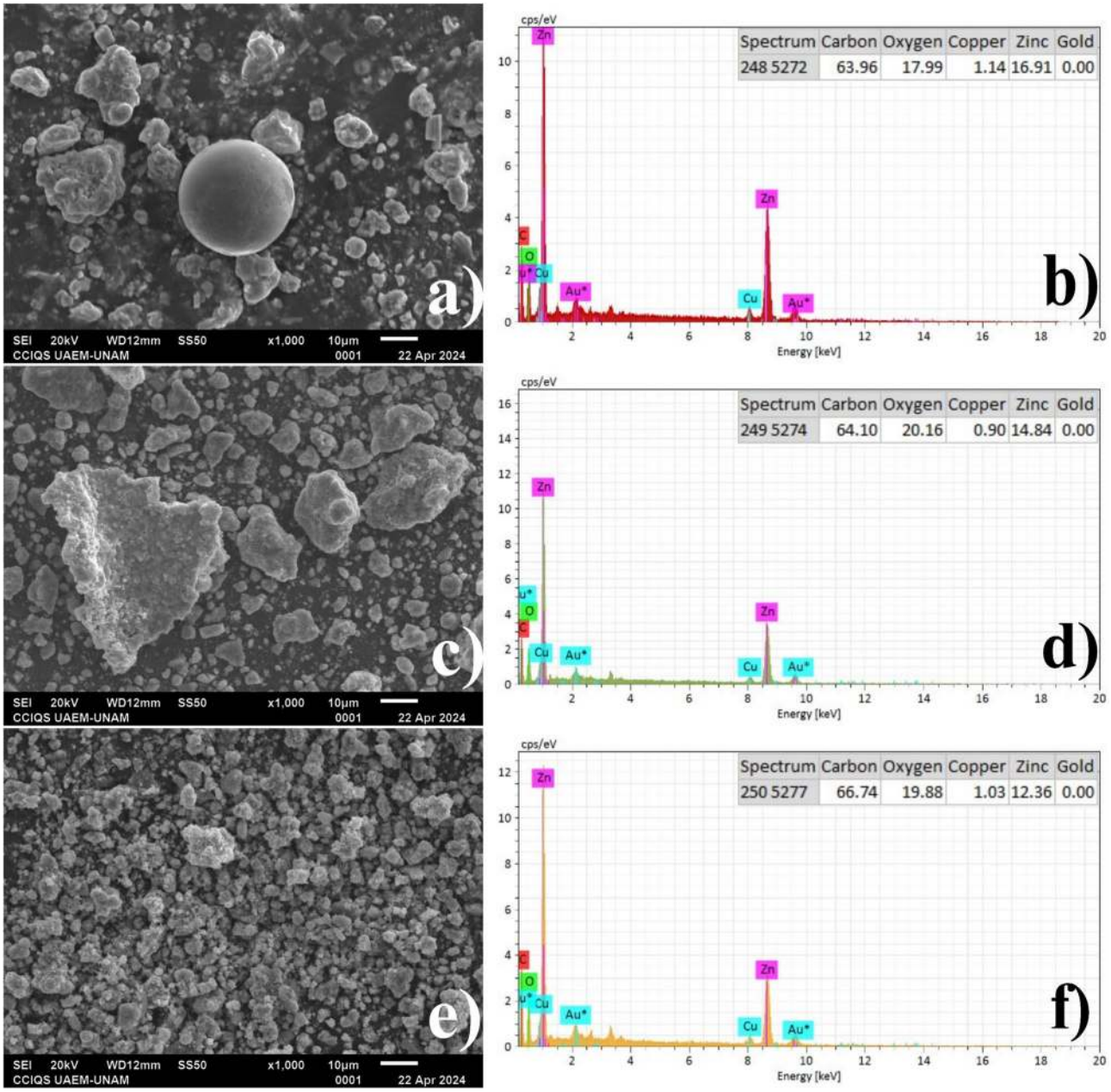


Fig. 4 SEM micrograph of **a** 1%-ZnO NPs, **c** 2%-ZnO NPs, and **e** 4%-ZnO NPs. Elemental composition of **b** 1%-ZnO NPs, **d** 2%-ZnO NPs, **f** 4%-ZnO NPs synthesized by green chemistry

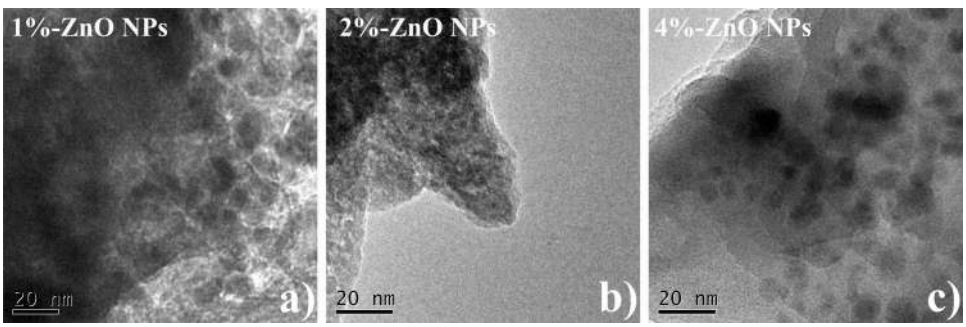


Fig. 5 TEM image of zinc oxide nanoparticles synthesized using cuachalalate bark extract **a** 1%-ZnO NPs, **b** 2%-ZnO NPs, and **c** 4%-ZnO NPs

31.77°, 34.42°, 36.25°, 47.54°, 56.60°, 62.85°, 66.38°, 67.95°, 69.09°, 72.56°, 76.96°, 81.38°, and 89.61°, which represent the (100), (002), (101), (102), (110), (103), (200), (112), (201), (004), (202), (104), and (203) crystallographic reflection planes of the hexagonal structure of mineral zincite, as stated in the Crystalline card JCPDS No. 01–089- 7102 [38]. A small peak around 2θ at a value of 30° may relate to the surface crystallization of organic constituents from the cuachalalate extract on the surfaces of the nanoparticles. The Debye–Scherrer equation was used to determine the average crystalline size.

$$D = \frac{K\lambda}{\beta \cos\theta} \tag{2}$$

D represents the size of the crystallite. The form factor, with a value of 0.9, is defined by K, which is the wavelength of the X-rays. It indicates the angle of incidence and describes the full width at half maximum (FWHM) of the diffraction peak located in the plane. The average crystallite dimensions (D) correspond to 21.6, 14.19, and 13.26 nm for 1%-ZnO NPs, 2%-ZnO NPs, and 4%-ZnO NPs. The results confirm the ZnO NPs crystalline structure and hexagonal phase. Furthermore, the intensity of the peaks can be used to observe the crystallinity of the nanoparticles. The presence of sharp, high-intensity peaks indicates high crystallinity. The crystallinity percentages for 1%-ZnO NPs, 2%-ZnO NPs, and 4%-ZnO NPs were calculated at 77, 83, and 86%, respectively. Results show that with an extended concentration of cuachalalate bark, there is a reduction in crystal size. Likewise, the width of the peak indicates a larger crystallite size; therefore, at a higher concentration, a smaller crystallite size and a major crystalline arrangement are observed [39–42].

3.4 Microscopic studies

The morphology of the ZnO NPs was observed in Fig. 4a–c. The particles show a variation of shapes and sizes, a non-uniform distribution, increased aggregation, loose aggregates, and a rough surface texture. The role of natural extracts in green synthesis, where molecules participate as stabilizers in forming ZnO NPs, is well known. In this case, the presence of

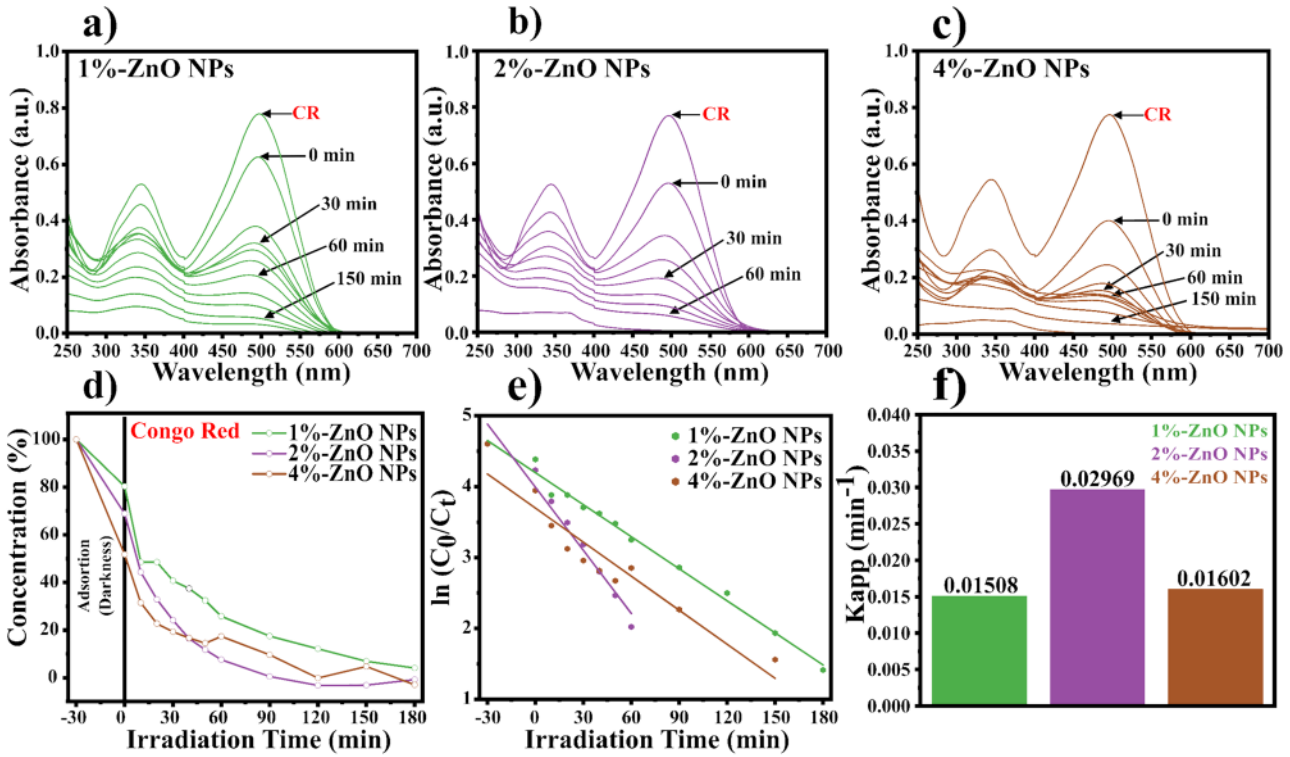


Fig. 6 Degradation spectra of Congo red using ZnO nanoparticles synthesized with *Amphipterygium adstringens* extract: 1%-ZnO NPs (**a**), 2%-ZnO NPs (**b**), and 4%-ZnO NPs (**c**). Graph comparing ZnO nanoparticles at different concentrations (**d**). Linear fitting of the pseudo first order kinetic model (**e**), and determination of the rate constant (**f**)

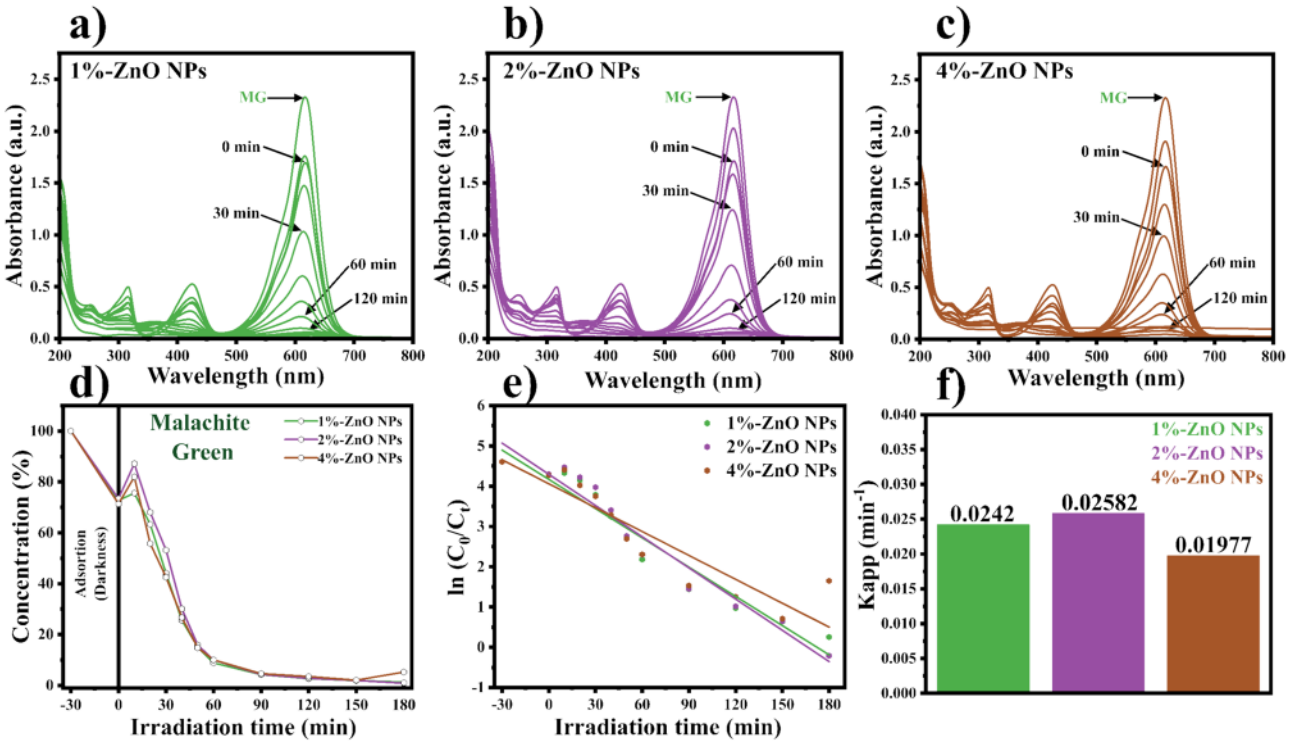


Fig. 7 Degradation spectra of Malachite green using ZnO nanoparticles synthesized with *Amphipterygium adstringens* extract: 1%-ZnO NPs (**a**), 2%-ZnO NPs (**b**), and 4%-ZnO NPs (**c**). Graph comparing ZnO nanoparticles at different concentrations (**d**). Linear fitting of the pseudo first order kinetic model (**e**), and determination of the rate constant (**f**)

natural molecules caused higher agglomeration as the concentration of cuachalalate increased. However, it can be observed in Fig. 4a that nanoparticles with a spherical shape are more separated from the rest; it is considered that a concentration of 1%-ZnO NPs provides a more uniform spherical structure with less accumulation due to the high surface energy they possess, which causes adhesion with greater frequency, resulting in larger clusters [43]. The EDS spectrum Fig. 4d–f, shows the chemical composition of the ZnO NPs. Three main chemical elements were detected in the EDS spectrum: zinc (Zn), oxygen (O), and carbon (C). They confirm the formation of ZnO. The carbon peak (C) may correspond to organic matter on the surface of the ZnO NP, as shown in the previous FTIR analysis (Fig. 2). This is attributed to the interaction of polyphenols as a capping agent [44].

The particle size was determined by TEM analysis. TEM analysis displayed a well-defined spherical structure, confirmed by SEM micrographs Fig. 5a–c. Moreover, the nanoparticles have lengths of about 10–20 nm, presenting a uniform structure among those synthesized with different concentrations of extracts. As reported in other studies, the extract acts as a capping agent in forming zinc oxide nanoparticles, stabilizing, size and shape. The agglomeration of the ZnO NPs is not visible due to the encapsulation of the ZnO NPs with cuachalalate bark extract. The bioactive constituents were observed due to polyphenols, alkaloids, and other compounds found in the cuachalalate [45–49].

4 Photocatalytic activity

The degradation of emerging pollutants, such as dyes and drugs, was studied under optimal experimental conditions, including the catalyst dose and the initial concentration of the contaminants. The decrease in absorbance can be observed as time elapses (the decay in color for dyes). The degradation percentage is also calculated using the initial and final absorbance values. In addition, the degradation rate was calculated using $\ln \frac{C}{C_0} = kt$ where C is concentration, t is time, C_0 is the initial concentration, and k is the rate constant corresponding to a first-order kinetic equation. This

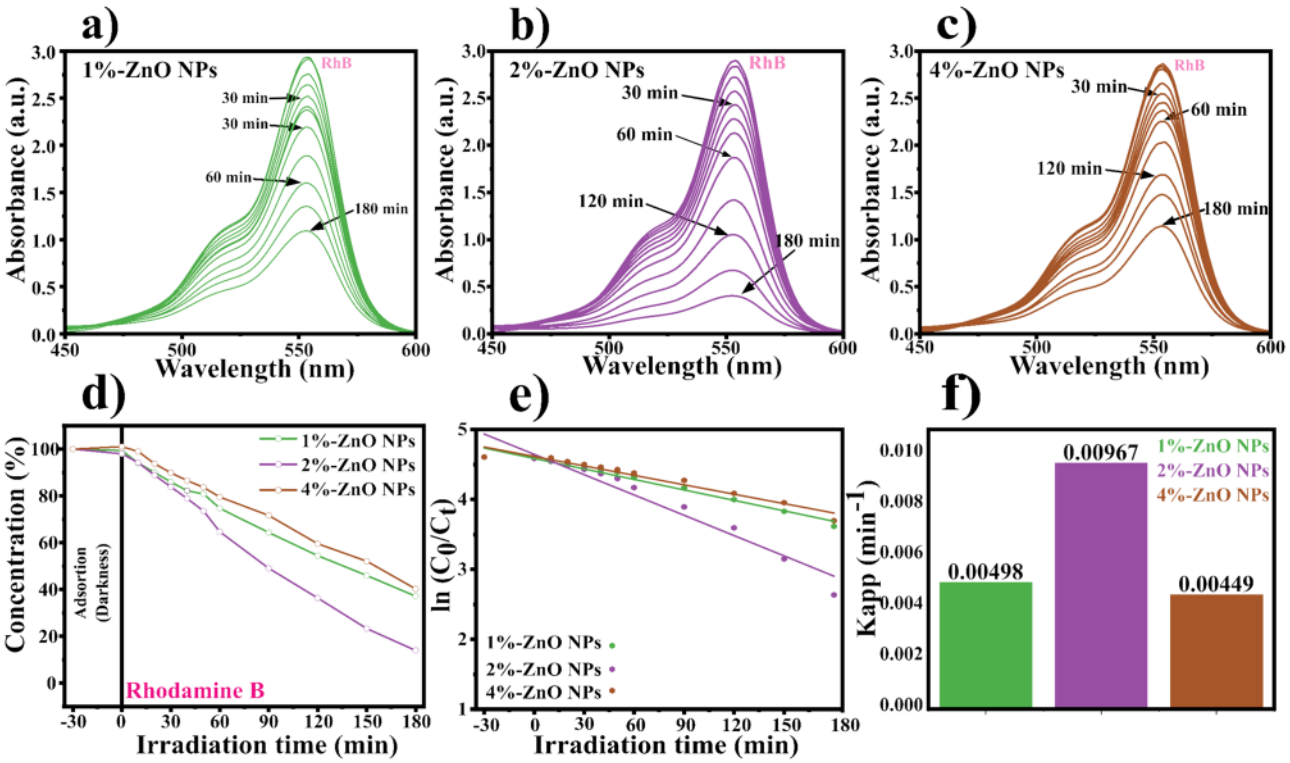


Fig. 8 Degradation spectra of Rhodamine B using ZnO nanoparticles synthesized with *Amphipterygium adstringens* extract: 1%-ZnO NPs (**a**), 2%-ZnO NPs (**b**), and 4%-ZnO NPs (**c**). Graph comparing ZnO nanoparticles at different concentrations (**d**). Linear fitting of the pseudo first order kinetic model (**e**), and determination of the rate constant (**f**)

experiment was carried out under exposure to UV irradiation for 180 min.

4.1 Colorants

4.1.1 Congo red (CR)

The photocatalytic activity was carried out with a zinc oxide semiconductor catalyst at a CR concentration of 15 ppm. It was observed in the UV spectrum Fig. 6a–c, that there was a decrease in absorbance over time, showing degradation of 96% for 1%-ZnO NPs, 100.8% for 2%-ZnO NPs, and 103% for 4%-ZnO NPs (Fig. 6d). It can be seen that the higher the concentration, the quicker the degradation rate (Fig. 6e, f). CR degradation is linked to the availability of more active sites on the photocatalyst surface, which increases the number of hydroxyl and superoxide radicals. However, catalyst accumulation decreases the degradation rate due to insufficient active sites [50–54].

4.1.2 Malachite green (MG)

Malachite green (MG) is a soluble cationic dye. It is a green crystalline powder of the triphenylmethane type. If present above a certain concentration level, it can contaminate surface and groundwater and pose potential health hazards to animals, plant life, and humans [55, 56].

The degradation of malachite green at a concentration of 15 ppm was carried out over the ZnO catalyst under UV light illumination for 180 min, with a 1:1 catalyst ratio. In Fig. 7a–c, the decreased absorbance over time indicates a decline in the concentration of MG dye. Additionally, Fig. 7d shows the concentration versus time graph, illustrating complete degradation in 180 min and demonstrating a stronger relationship between dark adsorption and complete mineralization. The rate constant value is calculated using a pseudo-first-order equation (Fig. 7e, f), indicating that the degradation efficiency values are consistent with the kinetic data. The degradation involves various processes, including the catalyst's active sites and the formation of hydroxyl radicals [57–62].

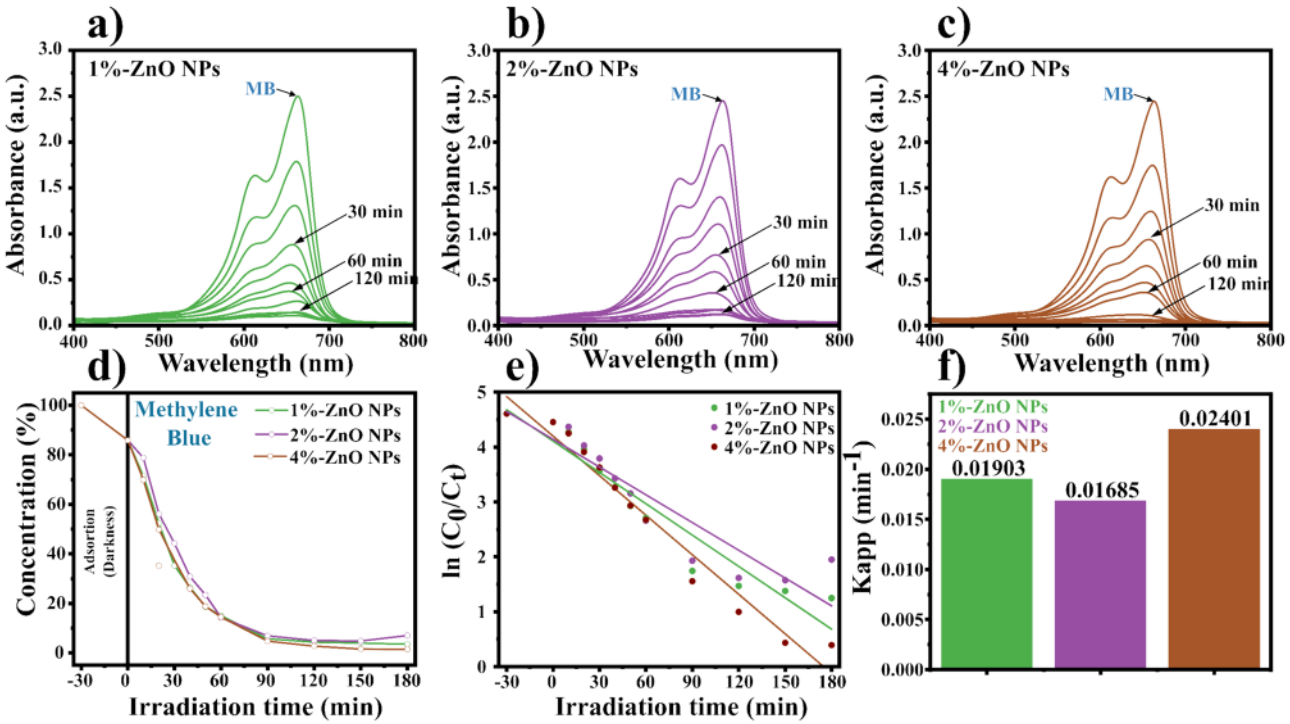


Fig. 9 Degradation spectra of Methylene blue using ZnO nanoparticles synthesized with *Amphipterygium adstringens* extract: 1%-ZnO NPs (**a**), 2%-ZnO NPs (**b**), and 4%-ZnO NPs (**c**). Graph comparing ZnO nanoparticles at different concentrations (**d**). Linear fitting of the pseudo first order kinetic model (**e**), and determination of the rate constant (**f**)

4.1.3 Rhodamine B (RhB)

On the other hand, Rhodamine B is one of the most challenging dyes to remove. Figure 8a–c, shows the absorption spectra of Rhodamine B over time, noting that the maximum absorption peak at 554 nm decreased during the photocatalytic degradation without the formation of byproducts or the appearance of other absorption bands. A decrease in the concentration of Rhodamine B (100%) resulted in concentrations of 40%, 37%, and 14% for 1%-ZnO NPs, 2%-ZnO NPs, and 4%-ZnO NPs over 180 min., culminating in partial mineralization [63–69].

4.1.4 Methylene blue (MB)

Methylene blue (MB) is a synthetic dye widely used as a colorant in paper and textiles. It is also used in large amounts in pharmaceuticals and self-care products. Therefore, MB solutions were used to study the photocatalytic degradation of ZnO, which was synthesized with different extract concentrations to understand the

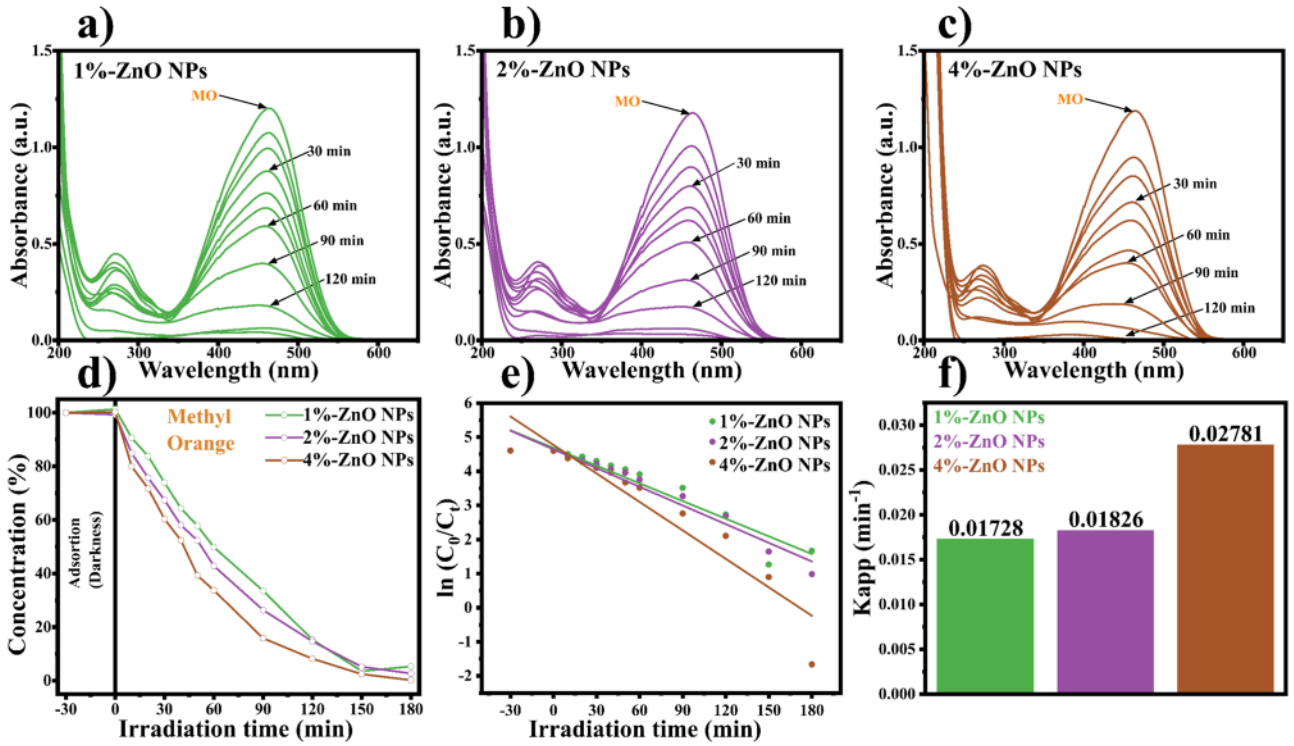


Fig. 10 Degradation spectra of Methyl orange using ZnO nanoparticles synthesized with *Amphipterygium adstringens* extract: 1%-ZnO NPs (**a**), 2%-ZnO NPs (**b**), and 4%-ZnO NPs (**c**). Graph comparing ZnO nanoparticles at different concentrations (**d**). Linear fitting of the pseudo first order kinetic model (**e**), and determination of the rate constant (**f**)

relationship between the structure and photocatalysis of ZnO NPs samples. The absorption peak at 664 nm is the typical peak of Methylene Blue. The loss of this peak in the sample indicates that MB was removed from the solution as CO_2 and H_2O. Figure 9a–c, show the absorbance measurement of the different extract concentrations in the synthesis of ZnO. The absorbance decreases with exposure to UV radiation over time. After 180 min of exposure to UV irradiation, the maximum concentrations achieved are 3.48% 1%-ZnO NPs 7% 2%-ZnO NPs and 1.47% 4%-ZnO NPs (Fig. 9d), indicating an almost complete degradation of the methylene blue dye. The rate constants were determined as 0.019 for 1%-ZnO NPs 0.0168 for 2%-ZnO NPs and 0.024 for 4%-ZnO NPs showing that a higher concentration and smaller size of nanoparticles indicate a faster degradation rate. Compared with Sedefoglu, 2023 reported various rate constants for different synthesis techniques through calcination: 0.0112, 0.02791, 0.3924, and 0.2332. This indicates that the same or better results can be obtained using green synthesis [70–78].

4.1.5 Methyl orange (MO)

Finally, the photocatalytic activity of the nanoparticles synthesized with cuachalalate bark extract was evaluated in methyl orange dye, a widely used dye with a less complex chemical structure commonly used in the textile industry. Figure 10a–c, shows the measurement of the UV spectrum, presenting an absorbance peak characteristic of methyl orange at a wavelength of 464 nm; as the exposure time increases, the spectrum decreases. After 180 min of exposure, it reached a degradation of the dye of 94.69% for 1%-ZnO NPs, 97.32% for 2%-ZnO NPs, and 99.81 for 4%-ZnO NPs, respectively (Fig. 10d). Correlating, the increase in the concentration of cuachalalate extract in the synthesis of zinc oxide nanoparticles increased the percentage of methyl orange degradation, reaching almost 100% mineralization. In addition, the rate constant (Fig. 10e, f) was obtained, showing a K value of 0.01728 for 1%-ZnO NPs, 0.01826 for 2%-ZnO NPs, and 0.02781 for 4%-ZnO NPs. This results in lower concentration and major rate degradation. In this case, the relationship between the surface catalyst and dye is not

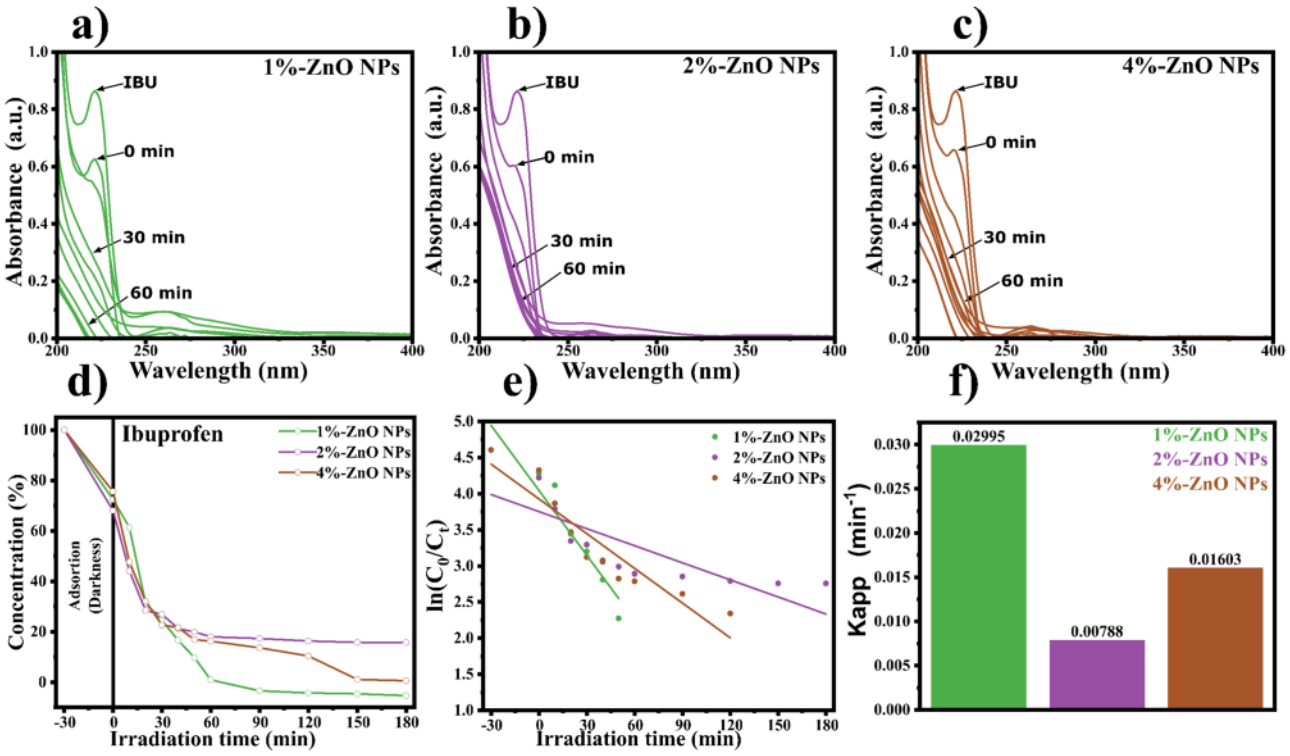


Fig. 11 Degradation spectra of Ibuprofen using ZnO nanoparticles synthesized with *Amphipterygium adstringens* extract: 1%-ZnO NPs (**a**), 2%-ZnO NPs (**b**), and 4%-ZnO NPs (**c**). Graph comparing ZnO nanoparticles at different concentrations (**d**). Linear fitting of the pseudo first order kinetic model (**e**), and determination of the rate constant (**f**)

perfect; eventually, prolonged exposure to UV irradiation is responsible for the central degradation of the dye [79–83].

4.2 Drugs

4.2.1 Ibuprofen (IBU)

Ibuprofen (IBU) is a non-steroidal anti-inflammatory drug with hydrophobic properties and low adsorption to organic matter. This drug was used as a model for its high-demand commercial. Figure 11a–c, displays the graph characteristic of ibuprofen, observing a peak of 221 nm corresponding to ibuprofen absorbance. The absorbance peak decreases as a function of the time it is prolonged. The degradation archived a percentage of 99% for 1%-ZnO NPs in 60 min and 99.45% for 4%-ZnO NPs in 180 min, ending the complete mineralization obtained H_2O and CO_2 at the end of the reaction. However, the degradation percentage was 84.23% for 2%-ZnO NPs in 180 min, achieving lower degradation over a more extended period (Fig. 11d). They reflect that the photocatalytic properties of the catalyst synthesized with 2%-ZnO NPs are lower than those at 1%-ZnO NPs and 4%-ZnO NPs. Therefore, the degradation constant k (cm^{-1}) was determined to compare with each other, obtaining a result of 0.029 for 1%-ZnO NPs, 0.0078 for 2%-ZnO NPs, and 0.016 for 4%-ZnO NPs. It is shown that using 2%-ZnO NPs can accelerate degradation, but it isn't finalized (Fig. 11e, f). This depends on the relationship between the adsorption sites on the surface of ZnO and the IBU and its by-product [84]. Figure 11d shows that 2%-ZnO NPs have more adsorption than the other two percentages of the extract, confirming those mentioned above; this can be due to reactive species ($\bullet O_2$, $\bullet OH$, and h^+) that participated in the degradation of IBU $\bullet O_2$ playing a critical role. These are possible active sites of IBP and the corresponding subsequent transformation products [85–91].

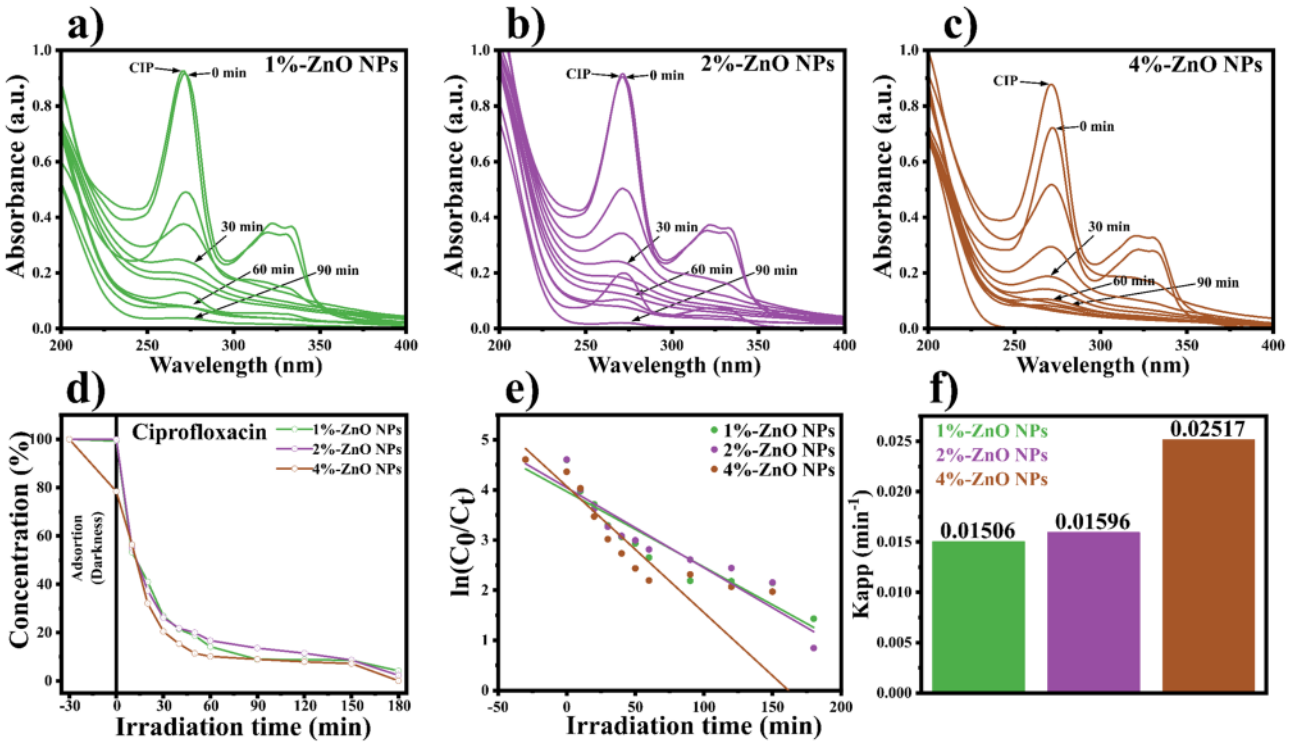


Fig. 12 Degradation spectra of Ciprofloxacin using ZnO nanoparticles synthesized with *Amphipterygium adstringens* extract: 1%-ZnO NPs (**a**), 2%-ZnO NPs (**b**), and 4%-ZnO NPs (**c**). Graph comparing ZnO nanoparticles at different concentrations (**d**). Linear fitting of the pseudo first order kinetic model (**e**), and determination of the rate constant (**f**)

4.2.2 Ciprofloxacin (CIP)

Ciprofloxacin is an antibiotic widely used for treating infections, but poor practices have increased its presence in wastewater, causing drug-resistant bacteria. Under UV irradiation, the photocatalytic degradation of CIP utilizing heterostructure ZnO catalysts was studied. Figure 12a–c, shows a maximum peak at 271 nm, corresponding to the spectral absorbance of CIP. The photocatalytic activity degraded by 85.83% for 1%-ZnO NPs, 97.66% for 2%-ZnO NPs, and 99.91% for 4%-ZnO NPs (Fig. 12d). Equilibrium adsorption–desorption is perfect, except that the synthesized catalyst, 4%-ZnO NPs, shows more promising adhesion to the catalyst surface. Following the degradation rate, the pseudo-first-order equation obtained a value k (cm^{-1}) of 0.01506 for 1%-ZnO NPs, 0.01596 for 2%-ZnO NPs, and 0.025 for 4%-ZnO NPs, respectively. This indicates that the synthesized catalyst, 4%-ZnO NPs, which demonstrated a significant degradation rate, results in complete mineralization. The degradation is proportional to the constant rate, meaning there is a lower

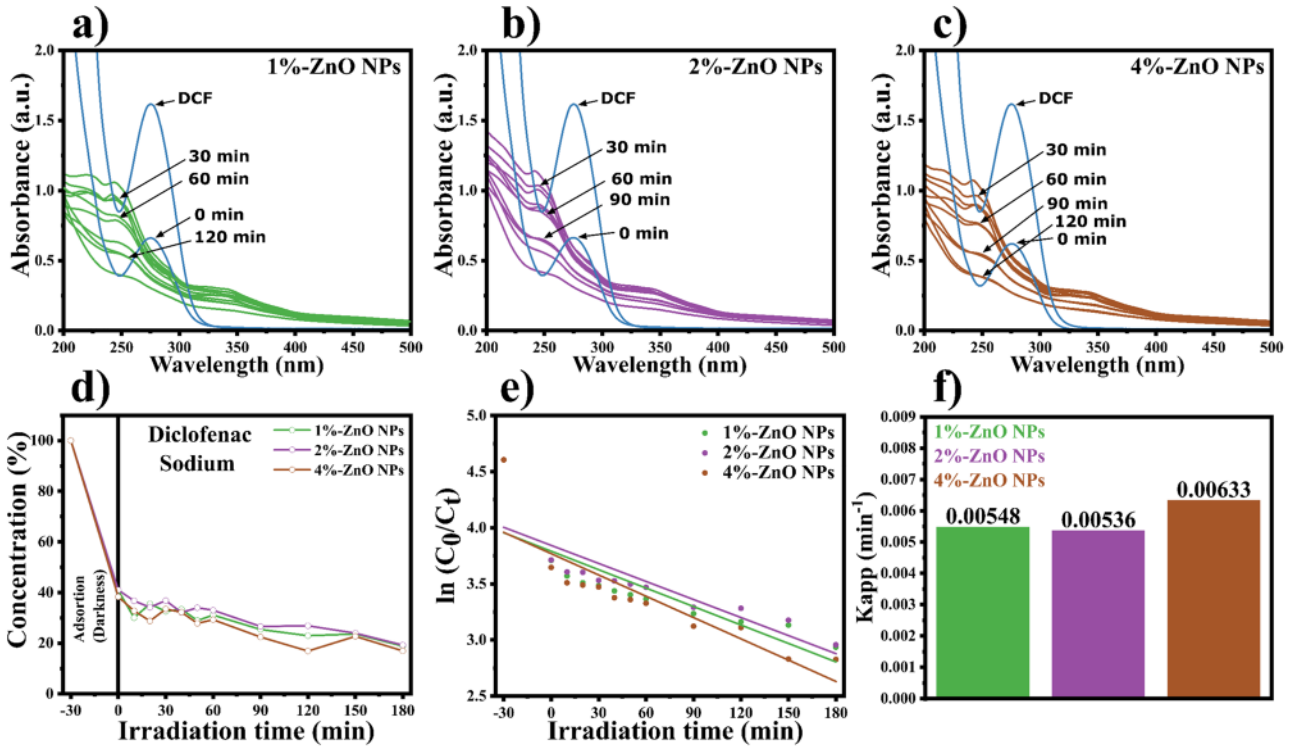


Fig. 13 Degradation spectra of Diclofenac sodium using ZnO nanoparticles synthesized with *Amphipterygium adstringens* extract: 1%- ZnO NPs (**a**), 2%-ZnO NPs (**b**), and 4%-ZnO NPs (**c**). Graph comparing ZnO nanoparticles at different concentrations (**d**). Linear fitting of the pseudo first order kinetic model (**e**), and determination of the rate constant (**f**)

percentage of degradation at a higher rate constant. The synthesis of the ZnO catalyst with 4%-ZnO NPs shows complete mineralization. However, the recombination of electron–hole pairs under UV irradiation contributes to the significant degradation of CIP due to the generation of three different types of radicals ($\bullet O_2$, $\bullet OH$, and h^+) that can be produced over a catalyst; however, only photogenerated O_2^- can diminish CIP [92–99].

4.2.3 *Diclofenac sodium (DCF)*

The diclofenac sodium has a behavior that is different from that of Ibuprofen and ciprofloxacin. Upon interaction with light, the drug begins to react and produce by-products; therefore, when performing absorbance measurements, a spectrum different from the original one can be observed Fig. 13a–c, the catalyst begins to interact and triggers a photocatalytic reaction carrying out the mineralization of the by-product formed. Figure 13d compares concentration with irradiation time, showing a final concentration of 81.18% for 1%-ZnO NPs, 80.77 for 2%-ZnO NPs, and 83.13% for 4%-ZnO NPs, respectively. The degradation rate can be observed in Fig. 13e, f. These phenomena result in the formation of very stable dimer carbazole. This by-subproduct turns a yellowish color, as reported by other authors, and a similar result was obtained in this experiment. From the first instant, the charge occurs to the by-subproduct molecule. The proposed pathway is carried out to form epoxide fact by including dissolved oxygen, followed by the loss of both chlorine atoms [100–106].

5 Conclusion

The degradation of pollutants in wastewater by functionalizing zinc oxide nanoparticles with *A. astringent* (cuachalalate) bark extract while applying green chemistry was successful. The characterization techniques indicated that the active compounds of the cuachalalate extract influenced the crystallite size,

crystallinity, morphology, and band gap, resulting in a zincite phase. Moreover, FTIR spectra confirmed that the nanomaterial contains high concentrations of organic molecules from the extract, which are part of the functionalization on the surface of the zinc oxide nanoparticles, increasing the photocatalytic activity of the material. The photocatalytic activity was tested on five dyes and three drugs, including ibuprofen, diclofenac sodium, and ciprofloxacin. Ibuprofen was successfully degraded, with a decrease in the aromatic ring (phenyl ring), removing 85% of IBU after 180 min. In the case of diclofenac sodium, the transformation of the original molecule into an intermediate can be observed upon interaction with light, showing an absorbance spectrum that differs from the original. However, photocatalysis removed more than 80% in 180 min. Finally, ciprofloxacin was degraded by over 90% after 180 min. These results indicate that the ZnO influenced by cuachalalate extract has extraordinary photocatalytic activity in eliminating dyes and drugs from the solution. It can be concluded that a significant part is the participation of hydroxyl radicals as the active agents responsible for the direct degradation of dyes and drugs.

Acknowledgements

The authors acknowledge Dr. Uvaldo Hernández and B.Sc. María Citlalit Martínez Soto for technical assistance during this work.

Author contributions

A. Moreno: investigation, methodology, and writing—original draft. A.R. Vilchis-Nestor: visualization, formal analysis and writing—review & editing. P.A. Luque: formal analysis, supervision, validation, and writing—review & editing.

Funding

The authors thank the projects of the Autonomous University of Baja California (UABC) 402/3391 and 402/3751, as well as 402/1/C/58/24. This research was funded by the Frontier Science Project with number 1805 of the Conahcyt.

Data availability

All data included in this study are available upon request by contact with the corresponding author.

Declarations

Conflicts of interest The authors declare that they have no known competing financial interests or personal relationships that could have appeared to influence the work reported in this paper.

Ethical approval This study does not involve experiments on human tissues.

Open Access This article is licensed under a Creative Commons Attribution 4.0 International License, which permits use, sharing, adaptation, distribution and reproduction in any medium or format, as long as you give appropriate credit to the original author(s) and the source, provide a link to the Creative Commons licence, and indicate if changes were made. The images or other third party material in this article are included in the article's Creative Commons licence, unless indicated otherwise in a credit line to the material. If material is not included in the article's Creative Commons licence and your intended use is not permitted by statutory regulation or exceeds the permitted use, you will need to obtain permission directly from the copyright holder. To view a copy of this licence, visit http://creativecommons.org/licenses/by/4.0/.

References

1. N.A. Ahammad, M.A. Ahmad, B.H. Hameed, A.T. Mohd Din, Environ. Sci. Pollut. Res. **30**, 124459 (2022)
2. M.P. Ajith, M. Aswathi, E. Priyadarshini, P. Rajamani, Bioresour. Technol. **342**, 126000 (2021)
3. M. Yasasve, M. Manjusha, D. Manojj, N.M. Hariharan, P. Sai Preethi, P. Asaithambi, N. Karmegam, M. Saravanan, Chemosphere **307**, 136017 (2022)
4. K. Jain, A.S. Patel, V.P. Pardhi, S.J.S. Flora, Molecules **26**, 1797 (2021)
5. Y. Liu, L. Zong, C. Zhang, W. Liu, A. Fakhri, V.K. Gupta, Surf. Interfaces **26**, 101292 (2021)
6. Y. Chen, A. Jihad, F. Hussam, S.H.Z. Al-Abdeen, J.M. Hussein, Z.H. Adhab, Z.H.A. Alzahraa, I. Ahmad, L. Fatolahi, B.J. Janani, Surf. Interfaces **38**, 102830 (2023)
7. R.K. Mishra, S.S. Mentha, Y. Misra, N. Dwivedi, Water-Energy Nexus **6**, 74 (2023)

8. J. Wang, J. Sun, J. Huang, A. Fakhri, V.K. Gupta, Mater. Chem. Phys. **272**, 124990 (2021)
9. A. Syed, A.M. Elgorban, A.H. Bahkali, R. Eswaramoorthy, M. Verma, R.S. Varma, B.J. Janani, J. Taiwan Inst. Chem. Eng. **149**, 105004 (2023)
10. A.A. Mahdi, R.A. Obeid, K. Abdullah, S. Mohammed, A.J. Kadhim, M.F. Ramadan, B.M. Hussien, A. Alkahtani, F.A. Ali, A.G. Alkhathami, L. Al-Fatolahi, A. Fakhri, Surf. Interfaces **40**, 102970 (2023)
11. A. Bahadoran, Q. Liu, B. Liu, J. Gu, D. Zhang, A. Fakhri, V.K. Gupta, J. Photochem. Photobiol. Chem. **416**, 113316 (2021)
12. I. Gehrke, A. Geiser, A. Somborn-Schulz, Nanotechnol. Sci. Appl. **8**, 1 (2015)
13. A. Kavitha, A. Doss, R.P. Praveen Pole, T.P.K. Pushpa Rani, R. Prasad, S. Satheesh, Biocatal. Agric. Biotechnol. **48**, 102654 (2023)
14. J. Prakash, H. Swart, Phys. B Condens. Matter **669**, 415297 (2023)
15. N. Hossain, M.H. Mobarak, M.A. Mimona, M.A. Islam, A. Hossain, F.T. Zohura, M.A. Chowdhury, Results Eng. **19**, 101347 (2023)
16. J. Gaur, S. Kumar, M. Pal, H. Kaur, K.M. Batoo, J.O. Momoh, Hybrid Adv. **5**, 100128 (2024)
17. N. Puri, A. Gupta, Environ. Res. **227**, 115786 (2023)
18. J. Jiang, J. Pi, J. Cai, Bioinorg. Chem. Appl. **1**, 2018 (2018)
19. I. Khan, K. Saeed, I. Khan, Arab. J. Chem. **12**, 908 (2019)
20. R. Mohammadipour-Nodoushan, S. Shekarriz, Z. Shariatinia, A. Heydari, M. Montazer, Int. J. Biol. Macromol. **242**, 124916 (2023)
21. A. Sirelkhatim, S. Mahmud, A. Seeni, N.H.M. Kaus, L.C. Ann, S.K.M. Bakhori, H. Hasan, D. Mohamad, Nano-Micro Lett. **7**, 219 (2015)
22. K. Muzammil, M. Zaid, U. Abdul-Reda Hussein, M.H. Abdul-jabbar, S.S. Jalal, M.A.A. Najm, M.Y. Alshahrani, A.F. Almulla, A. Alsaalamy, R.F. Amer, B.J. Janani, Mater. Sci. Semicond. Process. **168**, 107847 (2023)
23. K. Gayathri Devi, A. Clara Dhanemozhi, L. Sathya Priya, Mater. Today Proc. **34**, 1 (2023)
24. M. Karthik, C. Ragunath, P. Krishnasamy, D. Queen Paulraj, V. Ramasubramanian, Inorg. Chem. Commun. **157**, 111422 (2023)
25. Z. Azim, N.B. Singh, S. Khare, A. Singh, N. Amist, R.K. Yadav, Plant Nano Biol. **2**, 100011 (2022)
26. M. Sotelo-Barrera, M. Cília-García, M. Luna-Cavazos, J.L. Díaz-Núñez, A. Romero-Manzanares, R.M. Soto-Hernández, I. Castillo-Juárez, Plants **11**, 1766 (2022)
27. A. Rodriguez-Garcia, I.T.A. Peixoto, M.J. Verde-Star, S. De La Torre-Zavala, H. Aviles-Arnaut, A.L.T.G. Ruiz, Evid. Based Complement. Alternat. Med. (2015). https://doi.org/10.1155/2015/175497
28. C.V. Pérez-Contreras, J. Alvarado-Flores, A. Orona-Ortiz, J.L. Balderas-López, R.M. Salgado, N. Zacaula-Juárez, E. Krötzsch, A. Navarrete, J. Ethnopharmacol. **293**, 115313 (2022)
29. M.F. Islam, S. Islam, M.A.S. Miah, A.K.O. Huq, A.K. Saha, Z.J. Mou, M.M.H. Mondol, M.N.I. Bhuiyan, Heliyon **10**, e25430 (2024)
30. N. Ansari, A. Ali, M.S. Akhtar, S. Hasan, T. Khatoon, A.R. Khan, S.M. Wabaidur, Q.I. Rahman, Mater. Sci. Semicond. Process. **173**, 108087 (2024)
31. J. Jana, M. Ganguly, T. Pal, RSC Adv. **6**, 86174 (2016)
32. M.G. Arenas-Quevedo, J. Gracia-Fadrique, Chem. Thermodyn. Therm. Anal. **13**, 100128 (2024)
33. K. Vimala, S. Sundarraj, M. Paulpandi, S. Vengatesan, S. Kannan, Process Biochem. **49**, 160 (2014)
34. T.S. Aldeen, H.E. Ahmed Mohamed, M. Maaza, J. Phys. Chem. Solids **160**, 110313 (2022)
35. K. Rambabu, G. Bharath, F. Banat, P.L. Show, J. Hazard. Mater. **402**, 123560 (2021)
36. D. Torres-Ortiz, G. García-Alcocer, A.M. Loske, F. Fernández, E. Becerra-Becerra, R. Esparza, M.A. Gonzalez-Reyna, M. Estevez, Bioengineering **10**, 437 (2023)
37. M. Ramesh, M. Anbuvannan, G. Viruthagiri, Spectrochim. Acta. A. **136**, 864 (2015)
38. S. Easmin, M. Bhattacharyya, K. Pal, P. Das, R. Sahu, G. Nandi, S. Dewanjee, P. Paul, M.S. Haydar, S. Roy, T.K. Dua, Bioprocess Biosyst. Eng. **47**, 65 (2024)
39. M.Y. Al-darwesh, S.S. Ibrahim, M.A. Mohammed, Results Chem. **7**, 101368 (2024)
40. H. Chemingui, Environ. Technol. **45**, 926–944 (2022)
41. P. Perumal, Sci. Rep. **14**, 2204 (2024)
42. A. Raza, RSC Adv. **14**, 9799 (2024)
43. S. Nazneen, S. Sultana, Plant Sci. Arch. **176**, 129–140 (2024)
44. E. Hosseinzadeh, A. Foroumadi, L. Firoozpour, Inorg. Chem. Commun. **147**, 110243 (2023)
45. M. Saeed, L.A. Al-Keridis, S. Khattak, L. Alshuraym, N. Alshammari, H. Al-Amrah, T.K. Upadhyay, K.K. Kesari, Waste Biomass Valorization **15**, 5639 (2024)
46. B. Alallam, A.A. Doolaanea, M. Alfatama, V. Lim, Pharmaceuticals **16**, 269 (2023)
47. A.U.H. Khan, Y. Liu, C. Fang, R. Naidu, H.K. Shon, Z. Rogers, R. Dharmarajan, Environ. Adv. **12**, 100381 (2023)
48. F.M. Albarakaty, M.I. Alzaban, N.K. Alharbi, F.S. Bagrwan, A.R.M. Abd El-Aziz, M.A. Mahmoud, J. King Saud Univ. Sci. **35**, 102434 (2023)
49. X.-Q. Zhou, Z. Hayat, D.-D. Zhang, M.-Y. Li, S. Hu, Q. Wu, Y.-F. Cao, Y. Yuan, Processes **11**, 1193 (2023)
50. G.F. Aaga, S.T. Anshebo, Heliyon **9**, e16067 (2023)
51. R.S. Brishti, Md. Ahsan Habib, M.H. Ara, KMd. Rezaul Karim, Md. Khairul Islam, J. Naime, Md.M. Hasan Rumon, Md.A. Rayhan Khan, Results Chem. **7**, 101441 (2024)
52. S. Chakraborty, J.J. Farida, R. Simon, S. Kasthuri, N.L. Mary, Surf. Interfaces **19**, 100488 (2020)
53. J. Gaur, K. Vikrant, K.-H. Kim, S. Kumar, M. Pal, R. Badru, S. Masand, J. Momoh, Mater. Today Sustain. **22**, 100339 (2023)
54. W. Li, H. Li, Y. Yang, L. Liu, P. Wang, L. Xie, X. Chai, K. Xu, G. Du, L. Zhang, Ind. Crops Prod. **216**, 118753 (2024)
55. N.P. Raval, P.U. Shah, N.K. Shah, Appl Water Sci **7**, 3407 (2017)
56. S.J. Culp, F.A. Beland, J. Am. Coll. Toxicol. **15**, 219 (1996)
57. P.L. Meena, K. Poswal, A.K. Surela, Water Environ. J. **36**, 513 (2022)
58. S. Meena, D. Vaya, B.K. Das, Bull. Mater. Sci. **39**, 1735 (2016)
59. A. Modwi, M.A. Abbo, E.A. Hassan, O.K. Al-Duaij, A. Houas, J. Environ. Chem. Eng. **5**, 5954 (2017)
60. L. Saikia, D. Bhuyan, M. Saikia, B. Malakar, D.K. Dutta, P. Sengupta, Appl. Catal. Gen. **490**, 42 (2015)
61. S.N.A.M. Sukri, E.D.M. Isa, K. Shameli, IOP Conf. Ser. Mater. Sci. Eng. **808**, 012034 (2020)
62. R. Yadav, T.S. Chundawat, P. Rawat, G.K. Rao, D. Vaya, Bull. Mater. Sci. **44**, 250 (2021)
63. Y. Slimani, A. Khan, M. Nawaz, M.K. Hossain, A. Thakur, Spectrochim. Acta. A **321**, 124725 (2024)
64. A. Alshammari, A. Bagabas, M. Assulami, Arab. J. Chem. **12**, 1406 (2019)
65. K. El Akeb, H. Bessaha, H. Aguedal, M. Bouraada, B. Azambre, M.E.A. Elaissaoui Elmeliani, J. Water Process Eng. **65**, 105866 (2024)

66. S. Mancipe, J.J. Martínez, C. Pinzón, H. Rojas, D. Solis, R. Gómez, Catal. Today **372**, 191 (2021)
67. V.A. Mane, D.V. Dake, N.D. Raskar, R.B. Sonpir, M.D. Shirsat, B.N. Dole, Ceram. Int. **50**, 38871–38883 (2024)
68. N.M. Percivalle, M. Carofiglio, S. Hernández, V. Cauda, Discov. Nano **19**, 126 (2024)
69. A. Reynoso De La Garza, H. Zeghioud, A. Benítez-Rico, A. Romero-Nuñez, H. Djelal, T.E. Chávez-Miyauchi, J.Á. Guillén-Cervantes, Mater. Sci. Semicond. Process. **176**, 108349 (2024)
70. N. Sedefoglu, Optik **288**, 171217 (2023)
71. M.A. Ali, I.M. Maafa, I.Y. Qudsieh, Water **16**, 453 (2024)
72. E.A. Alzahrani, A. Nabi, M.R. Kamli, S.M. Albukhari, S.A. Althabaiti, S.A. Al-Harbi, I. Khan, M.A. Malik, Water **15**, 384 (2023)
73. A. Gharebaghi, A.H.J. Magham, L. Hokmabadi, Struct. Chem. **35**, 801 (2024)
74. S. Girma, A.M. Taddesse, Y. Bogale, Z. Bezu, J. Photochem. Photobiol. Chem. **444**, 114963 (2023)
75. S. Krobthong, T. Rungsawang, S. Wongrerkdee, Toxics **11**, 266 (2023)
76. L. Motelica, O.-C. Oprea, B.-S. Vasile, A. Ficai, D. Ficai, E. Andronescu, A.M. Holban, Int. J. Mol. Sci. **24**, 5677 (2023)
77. S. Muzammal, A. Ahmad, M. Sheraz, J. Kim, S. Ali, M.B. Hanif, I. Hussain, S. Pandiaraj, A. Alodhayb, M.S. Javed, H.A.Z. Al-bonsrulah, M. Motola, Energy Convers. Manag. **22**, 100547 (2024)
78. G.K. Weldegebrieal, H.H. Dube, A.K. Sibhatu, Int. J. Environ. Anal. Chem. **103**, 6146 (2023)
79. M. Asif, M. Shafiq, F. Imtiaz, S. Ahmed, A.A. Alazba, H.N. Hussain, F.N. Butt, S.A. Zainab, M.K. Khan, M. Bilal, Top. Catal. **67**, 1 (2024)
80. F. Ban, Y. Wei, J. Xin, C. Ye, A. Xiao, Chem. Sel. **9**, e202303252 (2024)
81. H. Laksaci, B. Belhamdi, O. Khelifi, A. Khelifi, M. Trari, Int. J. Environ. Sci. Technol. **21**, 7227 (2024)
82. Y. Song, S. Nie, H. Ji, T. Qin, Z. Ma, J. Clean. Prod. **467**, 142887 (2024)
83. Z. Tang, Y. Yang, W. Wei, Molecules **29**, 1817 (2024)
84. S. Pesik, E. Jobiliong, E. Steven, Int. Electron. Conf. Water Sci. **25**, 49 (2023)
85. N. Ahmadpour, M. Nowrouzi, V. Madadi Avargani, M.H. Sayadi, S. Zendehboudi, J. Water Process Eng. **57**, 104597 (2024)
86. L.V. Castro, M.E. Manriquez, E. Ortiz-Islas, G.M. Bahena-Gutierrez, React. Kinet. Mech. Catal. **136**, 1705 (2023)
87. Z. Feng, Front. Chem. **12**, 1424548 (2024)
88. M.W. Ibrahim, Y. Khane, Y.T. Mahmood, A. Schulz, H. Kosslick, Desalin. Water Treat. **320**, 100588 (2024)
89. Z.-B. Lv, J. Feng, R.-J. Zhao, J.-J. Shen, W.-W. Yang, Chemosphere **358**, 142106 (2024)
90. M. Rohan Khizer, Z. Saddique, M. Imran, A. Javaid, S. Latif, D. Mantzavinos, M. Momotko, G. Boczkaj, Sep. Purif. Technol. **350**, 127768 (2024)
91. M.C.R. Silva, S. Castro-Lopes, A.G. Jerônimo, R. Barbosa, A. Lins, P. Trigueiro, B.C. Viana, F.P. Araujo, J.A. Osajima, R.R. Peña-Garcia, Molecules **29**, 391 (2024)
92. A. Murugan, V. Thirumal, J. Kim, V. Siva, P. Kasinathan, A.A. Alothman, S. Mohammad, K. Selvakumar, J. Taiwan Inst. Chem. Eng. **161**, 105495 (2024)
93. S. Aghdasi, M. Shokri, Ab Imp. **6**, 481–487 (2016)
94. Y. Iqbal, S. Ahmed, M.H. Aziz, M. Alam, M. Asif, Q. Huang, Mater. Chem. Phys. **318**, 129299 (2024)
95. R.E. Núñez-Salas, A. Hernández-Ramírez, V. Santos-Lozano, L. Hinojosa-Reyes, J.L. Guzmán-Mar, M.Á. Gracia-Pinilla, M.D.L. Maya-Treviño, J. Photochem. Photobiol. Chem. **411**, 113186 (2021)
96. R.A. Putul, S.A. Fahim, SMd. Masum, Md.A.I. Molla, Int. J. Environ. Anal. Chem. **2024**, 1 (2024)
97. F. Tasleem, S. Manzoor, S. Tasleem, M. Khan, S.A. Khan, U. Nishan, N. Sabir, A.A. Khan, M. Imran, A. Badshah, M. Ahmad, R. Ullah, E.A. Ali, M. Soylak, Anal. Lett. **58**, 34 (2024)
98. L.M. Verma, A. Kumar, A.U. Bashir, U. Gangwar, P.P. Ingole, S. Sharma, Nanoscale Adv. **6**, 155 (2024)
99. M. Yousefi, M. Farzadkia, A.H. Mahvi, M. Kermani, M. Gholami, A. Esrafili, Chemosphere **349**, 140972 (2024)
100. R. Chadha, N. Kashid, D.V.S. Jain, J. Pharm. Biomed. Anal. **58**, 631 (2003)
101. S. Chianese, P. Iovino, V. Leone, D. Musmarra, M. Prisciandaro, Water Air Soil Pollut. **228**, 270 (2017)
102. D. Dhar, S.S. Basu, S. Sengupta, J. Environ. Chem. Eng. **12**, 112708 (2024)
103. M. Giahi, Russ. J. Appl. Chem. **88**, 2044 (2015)
104. C. Lara-Pérez, E. Leyva, B. Zermeño, I. Osorio, C. Montalvo, E. Moctezuma, Environ. Earth Sci. **79**, 277 (2020)
105. S. Latif, A. Liaqat, M. Imran, A. Javaid, N. Hussain, T. Jesionowski, M. Bilal, Environ. Res. **216**, 114500 (2023)
106. M. Tanveer, G.T. Guyer, G. Abbas, Water Environ. Res. **91**, 822 (2019)

Publisher's Note Springer Nature remains neutral with regard to jurisdictional claims in published maps and institutional affiliations.